MACROSCOPIC BEHAVIOR AND MICROSTRUCTURAL ANALYSIS OF RECYCLED AGGREGATE MORTAR BARS EXPOSED TO EXTERNAL SULFATE ATTACK

Lautaro R. Santillán[(1)]✉, Yury A. Villagrán Zaccardi[(2)], Claudio J. Zega[(3)], Esperanza Menéndez Méndez[(4)]

(1) IITCI CONICET-UNCo, Buenos Aires 1400, Neuquén (8300), Argentina (lrsantillan@conicet.gov.ar).
(2) Sustainable Materials, Flemish Institute for Technological Research (VITO), Boeretang 200, BE-2400 MOL, Belgium (yury.villagranzaccardi@vito.be).
(3) LEMIT, CONICET, Calle 52 s/n e/121 y 122, La Plata (1900), Argentina (cj.zega@conicet.gov.ar).
(4) Instituto de Ciencias de Construcción Eduardo Torroja (IETcc), C. de Serrano Galvache, 4, 28033 Madrid, Spain (emm@ietcc.csic.es).

Keywords: recycled concrete aggregate, sulfate attack, salt cristalization, expansion, thermal analyses

ABSTRACT

The performance of cementitious materials made with Recycled Concrete Aggregates (RCA) and exposed to sulfate-laden environments is not yet fully understood. There are few studies on this topic, and for a full description of the mechanisms of external sulfate attack (ESA), several influencing parameters should be considered. The replacement of natural aggregates by RCA modifies the physical and chemical properties of the new material and introduces additional variables into the already complex mechanism. The high porosity of RCA contributes to accelerating the sulfate penetration from the surface, while the attached mortar increases the mineral supply that can react with the incoming sulfate.
This paper describes a study on the performance of mortars made with RCA exposed to different ESA conditions. Design and exposure parameters include three cement, two specimen sizes, and two sulfate media (soil and solution). Visual inspection and measurements of expansion and weight change were used to determine the performance of the mixes. From a microstructural point of view, thermogravimetric analyses were carried out on samples obtained from the mortar bars after exposure. These results are then used to infer on the thermodynamic and kinetic aspects of ESA progression in recycled mortar. Finally, SEM/EDS analyses were also performed to further describe sulfate penetration and its relationship with cracking. The results show a limited influence of fine recycled aggregate on the mortar performance against ESA and no proportionality to its content.

1. INTRODUCTION

The production of concrete, one of the most used materials in the construction industry, causes significant environmental impacts. The concrete industry consumes a significant amount of non-renewable resources. Particularly in the case of aggregates, the depletion of resources through the exploitation of natural quarries is increasingly banned due to the impact on the landscape and the reduction of productive land. Moreover, the volume of concrete waste in landfills continues to increase. Thus, the use of concrete waste to produce aggregates for the production of new concrete is an environmentally friendly and viable practice, as it enables reductions in the mining of natural aggregate and landfilling of construction and demolition waste [1–6].

The use of recycled concrete aggregate (RCA) in the production of new concrete has been extensively studied for decades. Several reports have shown that the use of coarse RCA as a partial replacement of coarse natural aggregate has a limited effect on the mechanical properties of concrete [7–11]. It is known that the mortar attached to RCA particles increases the volume of the interfacial transition zone and the overall porosity of the new concrete [8,12–14]. These effects may affect the durability of recycled aggregate concrete, as transport properties are increased. Nevertheless, there is not a completed knowledge about the RCA effect in each type of exposition type, and some results in the literature are not consistent yet [15–20].

Regarding the specific case of external sulfate attack (ESA), there is limited literature that evaluates mixes with RCA [21–28], and these results are not entirely consistent. Some studies indicate a poorer performance of cement-based mixes with RCA [5,21,22,29,30], while others suggest a similar or even better performance of mixes with RCA [24,27,31,32].

It appears that other parameters of each different experimental campaign (materials, mixes proportioning, types of exposure, etc.) determine the effect of RCA on the ESA phenomenon. The study of ESA process involves many parameters, and the use of RCA introduces new variables that further complicate the assessment in a single experimental campaign. The use of RCA can negatively affect the performance of concrete or mortar exposed to sulfate-laden media for two main reasons: first, it increases concrete porosity, which may translate into an increase in the sulfate transport rate; second, attached mortar in RCA implies an additional supply of hydration products of Portland cement (including aluminates), which increases the reactivity with sulfates. In this sense, the subject deserves experimental studies to assess these potential effects. Finally, the higher porosity of RCA bearing mixes could play a positive role since it provides more free space for the accommodation of ESA products (buffer capacity) [33].

In addition, there are several proposed methods in the literature for the evaluation of ESA on concrete and mortar specimens. Macroscopic physical changes (e.g., length and weight variations, cracking) are the most widely used evaluation methods due to their practical implementation. However, these refer to volumetric properties, and as such they are unable to explain in depth the kinetics of the ESA process [34]. As ESA starts on the surface and progresses in depth with time, microstructural analysis and profiling are necessary to establish a correlation between macroscopic changes (length, weight, and cracking) and microscopic changes due to ESA [35–37]. Such information for RCA concrete and mortar is particularly lacking in the literature. Mineralogical changes produced by ESA can be assessed by techniques such as SEM/BSE, XRD, or TGA.

The type of exposure of samples can also influence the evaluation of the behavior of recycled mortars against ESA. The saturation state of samples during testing could determine the transport mechanism of the ions into the matrix, and the porosity involved in it. In a saturated state, the transport mechanism is diffusion, and the entire porosity is affected. In a non-saturated state, capillary absorption also has a participation rate, but only a part of the total porosity takes part [38–40]. In addition, in a non-saturated state, ESA is likely to be combined with physical sulfate attack (PSA), which is a particular form of salt crystallization [41–43]. The role of RCA may also change regarding the predominant attack mechanism, since it modifies the porosity system of the evaluated material and other related properties, such as mechanical strength and stiffness. The size and slenderness of specimens also have an effect on ESA progression [35,44], since the ESA and PSA have a superficial characteristic.

The present study provides results of experimental procedures with the aim of knowing, on the one hand, the influence of RCA on the ESA process and, on the other hand, assessing possible methods to evaluate the potential effect of RCA mortar under ESA. Mortar mixes with different contents of fine recycled aggregate (FRA) and cement types were prepared. Two specimen sizes were cast with each mortar and exposed to two conditions: immersion in sulfate solution, and burial in sulfate-rich soil. Common evaluation methods, such as length and weight changes and visual inspection, were used to determine the ESA-related damage on samples. In addition, microstructural analyses were performed to determine the effects of the variables considered on the test results and confirm the macroscopic changes observed.

2. METHODOLOGY

2.1. Materials and specimens

Three types of Portland cement were used in this study: a low C_3A Ordinary Portland cement (O) (equivalent to CEM I 42.5 N, EN 197-1); a low-C_3A limestone-blended Portland cement (L) (equivalent to CEM II/A-L 42.5 N, EN 197-1); and a high-C_3A limestone-blended Portland cement (H) (equivalent to CEM II/A-L 52.5 N, EN 197-1). Table 1 summarizes the chemical and mineralogical compositions of the cements as determined by XRF and Rietveld analyses [45], respectively.

Table 1 - Chemical and mineralogical compositions of cements.

Cem.	CaO	SiO_2	Al_2O_3	Fe_2O_3	SO_3	C_3S	C_2S	C_3A	C_4AF	C	G	LF
O	64.2	18.9	3.7	2.9	2.3	18	56	4.9	8.8	87.7	4.9	4.2
L	65.8	18.8	3.1	3.0	1.9	13	41	3.2	7.8	65.0	3.9	22.0
H	65.9	19.2	3.6	0.1	2.6	18	50	9.4	0.5	77.9	3.7	17.2

C: Total clinker; G: Gypsum; LF: Limestone Filler

The fine recycled aggregate (FRA) was obtained from crushing waste concrete with a compressive strength of 25 MPa (i.e., structural concrete). Natural river siliceous sand (NS) and manufactured sand (crushed granite) (CGS) were used as fine aggregates. Table 2 presents the properties of the fine aggregates used.

Table 2 – Properties of fine aggregates.

Sand	Water Absorption, (%)	Fineness modulus	Density, (gr/cm^3)
NS	0.4	1.06	2.65
CGS	0.6	3.59	2.69
FRA	5.8	3.55	2.30

Table 3 presents the mix proportions for each mortar. FRA mixes contained 30 or 50 % vol. of FRA with respect to the total volume of fine aggregate, with the remainder being NS. The control mixes were made with 30 % vol. CGS and NS for the rest. Each mix is labelled with a letter indicating the constituting cement and a number indicating the FRA relative content.

The mortars were designed with a water-to-cement ratio of 0.45, a value usually recommended for producing sufficiently durable concrete. For the FRA mortars, mixing water content was adjusted by adding an amount equal to 50% of the FRA's water absorption capacity. A dose of superplasticizer was added in all mixes to obtain good flowability, using the same admixture in 1% of the weight of cement. This resulted in minor variations in the flowability of mixes, but in all cases, the workability was sufficient for proper casting and compaction in the molds. A standard high energy compaction procedure with a jolting table was applied to all samples, and the variations in consistency did not result in variations of the degree of compaction.

Table 3 - Proportions of mortars (g).

Mortar ID	Cement	Water	NS	CGS	FRA
O-0	1000	450	1806	774	-
O-30	1000	477	1806	-	669
O-50	1000	495	1280	-	1135
L-0	1000	450	1806	774	-
L-30	1000	477	1806	-	669
L-50	1000	495	1280	-	1135
H-0	1000	450	1806	774	-
H-30	1000	477	1806	-	669
H-50	1000	495	1280	-	1135

For each mortar, six prisms of 25 x 25 x 285 mm^3 (long bars) and six prisms of 40 x 40 x 160 mm^3 (short bars) were made for length and weight measurements. Additionally, three prisms of 40 x 40 x 160 mm^3 were cast to determine flexural and compressive strengths. All specimens were cured in lime-saturated water at a temperature of 23 ± 2 °C for 28 days. The specimens used for evaluating expansion and weight variation were sealed with epoxy paint at their ends (the surface around the pins) to prevent attack near the pins. After the paint had hardened, they were once again saturated in lime water for 72 hours before the initial measurements and exposure to sulfates. The flexural and compressive strength were evaluated following the Argentinean Standard IRAM 1622 [46] (similar to ASTM C 438 and ASTM C 109). The water absorption and density (with 3 samples per mix) were evaluated using the unaffected remaining pieces after the mechanical tests.

2.2. Exposure conditions and measurements

For each type of mortar and specimen size, the six bars (three per group) were exposed to two different conditions, both corresponding to very aggressive environments as described in ACI 318-14 [47]. The first group was buried in 2 g of Na_2SO_4/100 g of soil, with a mortar-to-soil volume ratio of 1:3. The soil vats were stored at ambient temperature (varying between 15 and 25 °C), and the internal relative humidity was always above 80%. The second group was immersed in 50 g/L Na_2SO_4 solution that was kept at 20 ± 2 °C and pH at 6-8, with periodic corrections with diluted sulfuric acid added after each measurement as necessary.

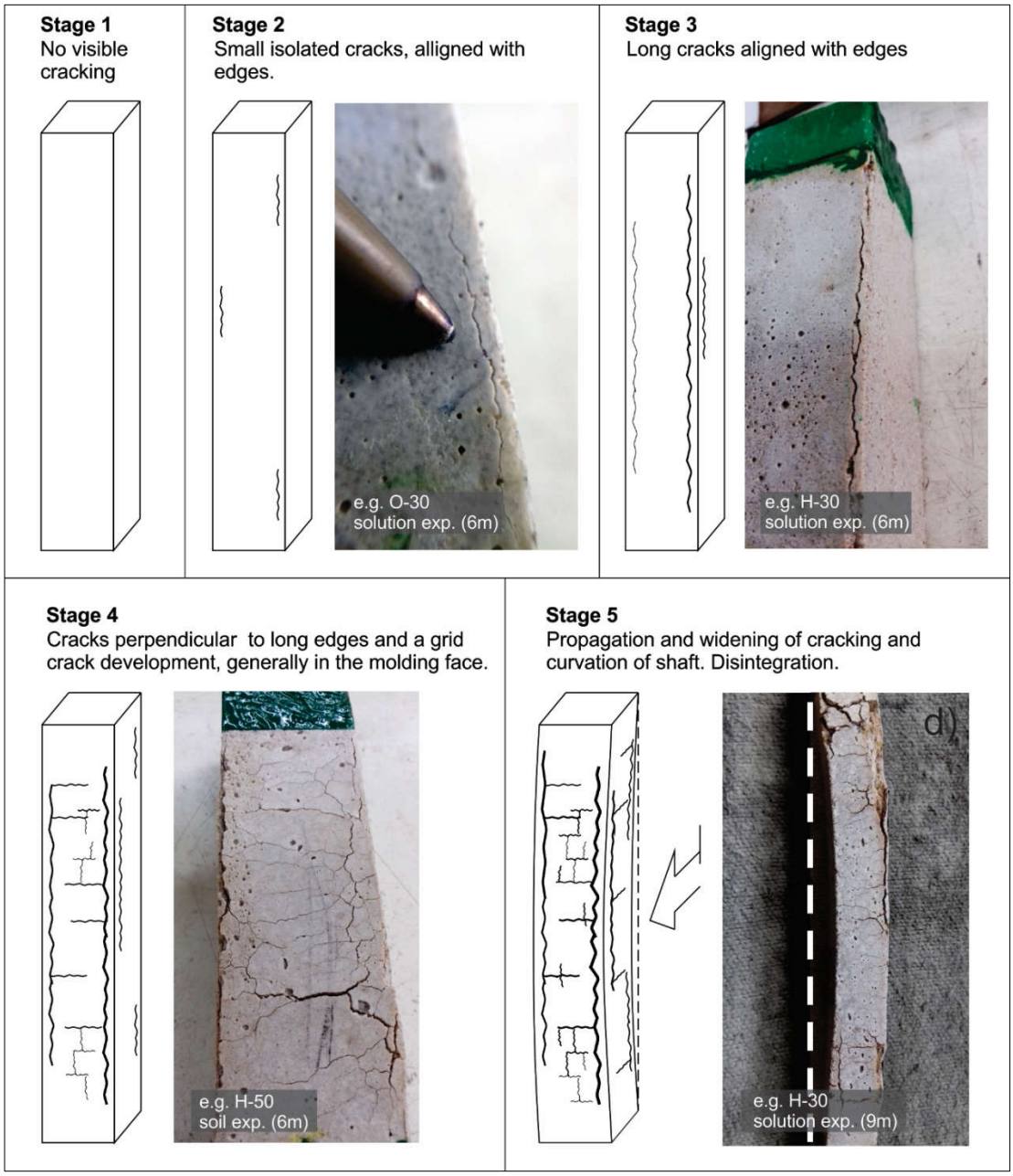

Figure 1 – Stages of ESA progression.

All mortar bars were evaluated by means of length and weight variations after exposure periods of 0, 7, 14, 28 days, and every month up to 1 year of exposure. For the purpose of visual inspection, five stages of ESA progression were stated, as indicated in Figure 1. With each measurement, each specimen was qualified visually and classified in the corresponding stage (it was considered that a group reached each stage when 2 of the 3 specimens in the group reached that stage).

2.3. Samples extraction and instrumental analysis

For the thermogravimetric analyses, a representative specimen was selected for each series, and two samples were collected manually as shown in Figure 2. For each mortar specimen, both bulk and surface samples were mechanically grounded and immediately evaluated using a NIEZTCH Jupiter device (from 20 to 1050 °C at 10 °C/min in an N_2 atmosphere). TG and DTG curves were analyzed to quantify compositions. Furthermore, polished section samples were prepared from the middle-part of the same representative mortar bars, and analyzed with scanning electron microscopy with energy dispersive X-ray spectroscopy (SEM/EDX).

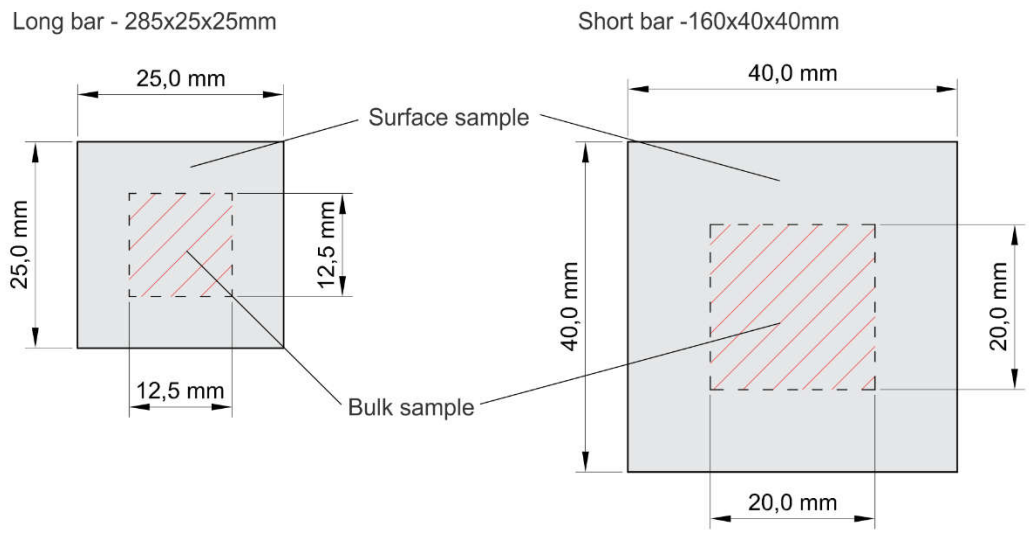

Figure 2 – Extraction of samples for TG analysis

2.4. Thermogravimetric quantitative analysis

Thermogravimetric analyses were performed on samples of representative long bars of the O, L, and H series for both expositions (solution and soil). Short bars of the H series were also analyzed by this method to observe the effect of size. Figure 3.a shows an example of DTG curves collected (bulk sample and surface sample) and the characteristic peaks analyzed. These peaks are related to the weight loss caused by dehydration, dehydroxylation, decarbonation, or decomposition of cement hydrates and ESA products. In the range measured, all samples showed peaks at similar locations due to the loss of weight. In the range of 50 to 200 °C, there is a significant overlap of peaks, including the decompositions of ettringite and gypsum (100 to 150 °C), hydrogarnet (around 140 °C), and AFm phases (multiple peaks between 60 and 200 °C). Moreover, C-S-H contributed to weight loss due to dehydration (65 to 600 °C, approximately). Later on, there are two isolated peaks corresponding to the

dehydroxylation of portlandite (400 and 480 °C) and the decomposition of carbonates (660 and 780 °C). The slight deviations from the temperature ranges normally reported for these phases are explained by variations in the fineness and amount of the tested sample. The ESA process is expected to consume portlandite to form gypsum and ettringite. Moreover, the carbonation process also consumes portlandite to form carbonates. Calcite and portlandite contents might also be affected by the FRA content, due to its attached cement paste.

The tangential method was used for the quantification of mineral phases, as described in [48]. This method involves measuring the area of the corresponding peak in the DTG curve. For this purpose, the onset and the end of each peak were discerned from the abrupt change in the curvature of the curves, and a straight line was drawn connecting these two-points, as shown in Figure 3.b. The enclosed region was calculated by integrating the area beneath the secant and substracting the area below the DTG curve in the temperature domain. This quantifies the loss of water or CO_2 (depending on the phase under analysis), and stoichiometric calculations were used to estimate the total amount of each phase. This methodology reduces the error in quantification due to substantial peak overlap in that the temperature range as opposed to the computations based on the full weight loss step within a given temperature range. It primarily allows for the decoupling of the phases of interest from the dehydration of C-S-H. It should be noted that the quantifications were made for samples with a high content of aggregates, which has the advantage of being more representative of concrete in service, but the disadvantage of significant dilution of phases of interest. Regardless, the outcome achieved and subsequently evaluated enables a beneficial comparative analysis among the various samples in view of their corresponding composition.

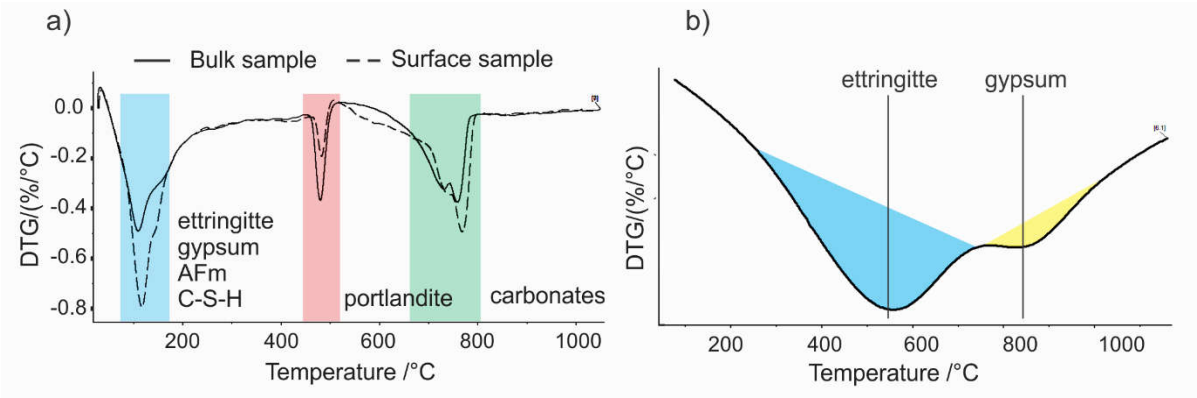

Figure 3 – Peak identification and quantification procedure based on DTG curves: a) examples of DTG curves and characteristic peaks, a bulk sample (solid line) and a surface sample (dashed line); b) tangential method for the quantification.

The selection of tangent points varied across the samples, with some showing shifts in the temperature range for the characteristic peaks due to methodological testing parameters such as sample size and fineness. Typically, ettringite was quantified in the range of 90-135 °C, corresponding to the highest first peak observed in this temperature range. The gypsum peaks were substantially overlapped by other dominant peaks (i.e., ettringite, alumina phases, C-S-H), hence the quantification (potentially underestimated) was considered within the visibly identifiable peak range of 130-170 °C. Portlandite was quantified in well-defined peaks that commonly fell within the range of 420-480 °C, and carbonates were primarily quantified within the range of 600-800 °C.

3. MACROSCOPIC RESULTS

3.1. Hardened properties

Table 4 presents the flow values in the fresh state, as well as the hardened properties evaluated at 28 days for mortars. An effect of the FRA content on flowability of mixes is observed. The high water absorption of FRA reduces the free water content, thereby affecting mortar mobility. Slightly lower flow values in the fresh state were obtained for H mortars, which can be explained by a greater water demand by the H cement due to its greater fineness compared to other cements. However, similar compaction degrees were achieved with the standard compaction procedure applied. Therefore, no impact on the hardened properties due to the consistency of mixes is noticed, i.e. comparable values for the density and water absorption.

Regarding these hardened properties, the main observed effect is from the FRA. As FRA increase, strength and density decrease, while water absorption increase. These results are in agreement with the literature [15,49]. The increase in porosity can be attributed to the inherent porosity of the FRA. Also, the lower flow values in FRA bearing mixes could induce porosity due to the presence of air-entrapped voids. However, the observed differences in flow values did not appear to significantly affect the compactness of the hardened mortars (compressive strength and density). This is possible since all mortars showed sufficient workability and were consistently compacted.

Table 4: Fresh and hardened properties of mortars (at 28 days).

Mortar ID	Flow [%]	Flexural strength [MPa]	Compressive strength [MPa]	24h water absorption [%]	Density [kg/dm^3]
O-0	109	8.1	53.0	7.5	2.08
O-30	95	8.4	52.1	9.4	1.97
O-50	85	8.4	47.3	10.9	1.91
L-0	108	7.1	40.0	7.2	2.08
L-30	107	7.3	42.1	9.1	1.97
L-50	111	7.6	42.4	10.5	1.94
H-0	82	7.0	48.6	7.8	2.09
H-30	84	7.1	46.2	9.1	2.04
H-50	81	7.5	44.9	9.8	2.00

3.2. Solution-exposed bars

Figure 4 shows the average expansions (solid lines) and weight changes (dashed lines) for each series of long and short mortar bars during 1 year of exposure to sulfate solution. The results show a main effect of the cement type of the recycled mortar on the final expansion of mortar bars and a secondary effect of the slenderness of the specimen. Only H mortars reached the propagation stage of ESA. FRA content shows a significant effect only for mortars with a low-performance matrix (H mortars).

For long bars, the L and O mortars had average expansions of less than 0.1%. This is the maximum limit after 1 year for compliance with ASTM C1012 [50] and is consistent with their

low-C_3A cement. In contrast, H mortar bars had average expansions up to three times this value (0.35, 0.85, and 0.42 % for 0, 30, and 50% FRA contents, respectively).

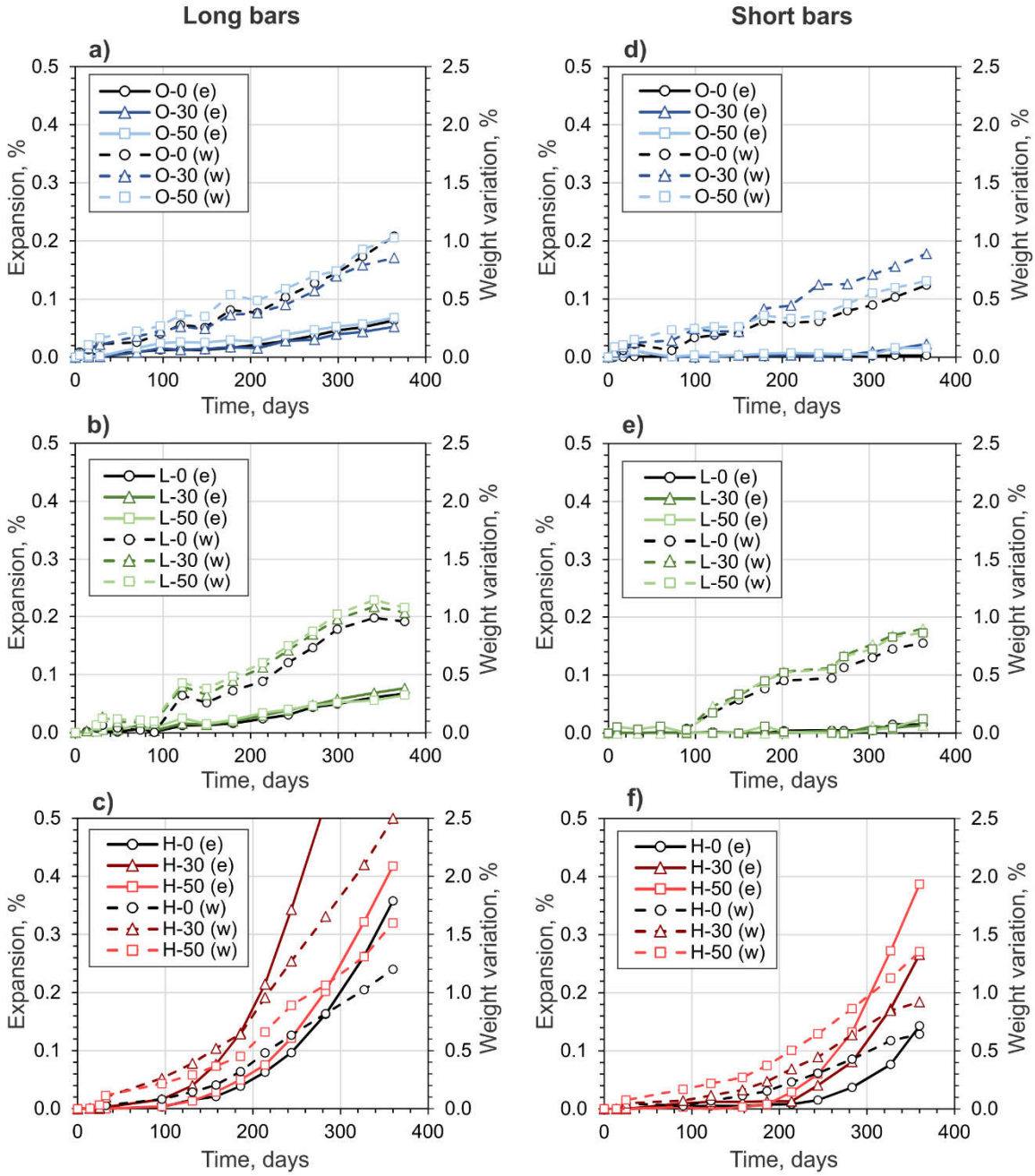

Figure 4 – Expansion (solid line) and weight variation (dashed line) of mortar bars immersed in sulfate solution: (a), (b), and (c), long bars of mortar series O, L and H, respectively; (d), (e), and (f), short bars of mortar series O, L, and H, respectively.

For short bars, the average expansions in O and L mortars were less than 0.02% (effect of slenderness), but for H mortar, the expansions were 0.12, 0.26, and 0.40%, for 0, 30, and 50% FRA contents, respectively. In all cases, the average weight change showed a good correlation

with the average expansion, supporting the correlation between the precipitation of ESA products and expansion.

Short bars had lower expansion values than long bars, as expected, but weight changes were similar for both bar types. This is due to the fact that both specimen types have approximately the same exposed surface area (260 cm^2 for long bars versus 224 cm^2 for short bars) but different cross-sectional areas. The expansion of mortar bars is correlated with the ratio between the sample volume under attack and the total volume of specimen [51], and this ratio decreases with decreasing slenderness. Moreover, a longer ESA induction period is observed for short bars compared to long bars for H mortars (~200 days for short bars and ~100 days for long bars).

The results also show that the FRA content has an influence on mortar expansion only when the cement of the new matrix has a high C_3A content (> 8 wt.%). However, the extent of this influence depended on the slenderness of the bars. For long bars, the H-30 mortar showed higher expansion than the H-50 mortar, while for short bars, the H-50 mortar showed a higher expansion than the H-30 mortar. The weight changes are consistent with these trends. The results suggest that the cross section of the specimen changes the pessimum value for the FRA content in mortar under ESA. This ambiguous effect of recycled aggregates on mortars performance has been earlier reported in the literature [24,31,52], although it seems to be influenced by other variables of the experimental set-up (see Section 5 for more details).

3.3. Soil-exposed bars

Figure 5 shows the corresponding results of average expansions (solid lines) and weight changes (dashed lines) for mortar bars buried in sulfate-rich soil. All values increased compared to the corresponding specimens in sulfate solution, which can be attributed to the effect of PSA. As with the sulfate solution, the cement type was critical to the behavior of the mortars, and only the mortars of the H series showed a propagation of ESA. Also, effects of slenderness and FRA content were observed in a second order. There is a good correlation between the expansion and the weight change, confirming the process of expansion by precipitation of ESA products inside the specimens.

For long bars, values above 0.1 % (limit criteria of ASTM C1012) are observed after 1 year of exposure, even for mortars made with low-C_3A cements. This can be attributed to the development of PSA, which is a physical attack and does not depend on the C_3A content of the cement. However, the H mortars still suffered significantly greater expansion than the O and L mortars, confirming a combination of salt crystallization and ESA that may produce a synergistic attack mechanism. In fact, the deterioration of the specimens was quite severe, and some specimens of the H mortars were destroyed even before 1 year of exposure was completed.

The size of the specimens played a similar role to the sulfate-solution exposure. For long bars, the O and L mortar bars expanded about 0.1% after 1 year of exposure, whereas for short bars, expansions were lower than 0.05%. For the O mortars, short bars showed a lower expansion and weight change than long bars. For the L mortars, short bars expanded less but showed a similar weight change to that of long bars. For H mortars, a small reduction in the propagation rate was observed in short bars, but the high damage observed for both sizes makes this difference irrelevant.

In this case, slight and inconsistent effects of FRA are observed in low-C_3A cement mortars and are attributed to its effect on porosity. For long bars, the O and L mortars with FRA showed the same or slightly lower expansions, while for short bars the effect was reversed. Weight variations were also higher for short bars when FRA was used, except for long bars made with O mortar, where the opposite effect occurred. In H mortars, the FRA content changed the duration of the induction period (~100 days for H-30 and H-50, and ~150 days for H-0).

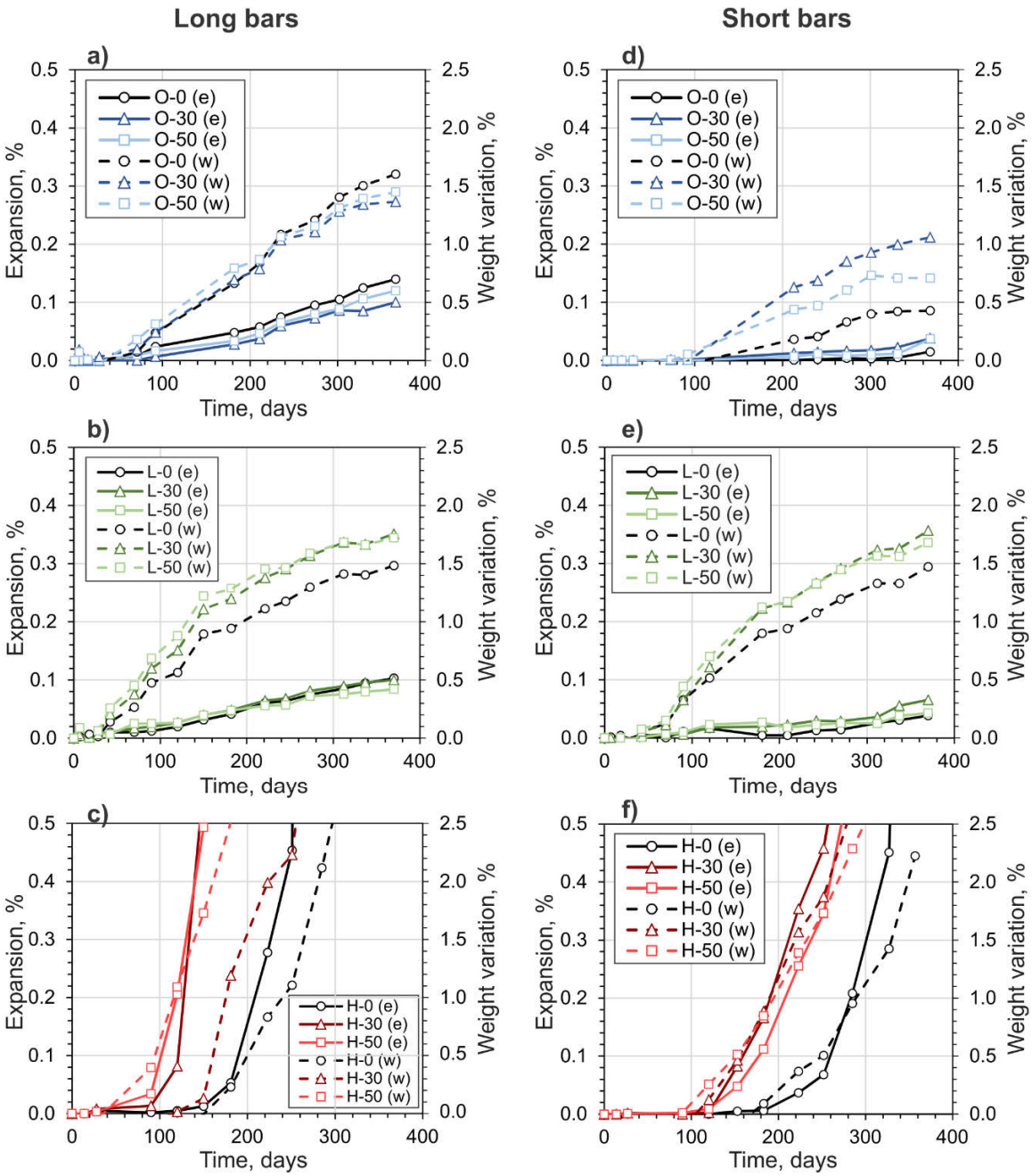

Figure 5 – Expansion (solid line) and weight variation (dashed line) for mortar bars buried in sulfate soil: (a), (b), and (c), long bars of the O, L, and H mortar series, respectively; (d), (e), and (f), short bars of the O, L, and H mortar series, respectively.

When analyzing the results from sulfate soil exposure, it should be mentioned that the standard deviations were higher than when exposed to sulfate solution (they were not plotted to maintain readability in the graph). The level of damage is more variable, which is probably due to local defects in the mortar bars that allow PSA to open cracks faster and trigger the expansion period. It can be summarized that the content of FRA was only significant in a poor chemical quality cement matrix, reducing the sulfate resistance of mixes. No results on mortars with recycled aggregates under these exposure conditions were not found in the literature. However, these findings align with results of concretes in comparable exposure conditions [30,31].

3.4. Visual inspection of damage

The results of the visual inspection are presented in Figure 6. There is a strong correlation between the length and weight changes and the progression of deterioration stages. On the one hand, long bars showed a higher degradation than short bars for the same exposure type. On the other hand, same size specimens were more damaged when exposed to the sulfate soil (ESA+PSA). Only H mortars reached stages 4 and 5 of damage. The time to reach stage 4 for each series had a good correlation with the time of the induction period observed in expansion and weight variation curves. Finally, a slight increment of cracking development is observed in soil-exposed samples of series O and L when they have a FRA replacement. This difference can be attributed to the higher porosity of FRA. This increased porosity results in higher transport properties, which can accelerate the PSA action, regardless of the cement type of the new matrix.

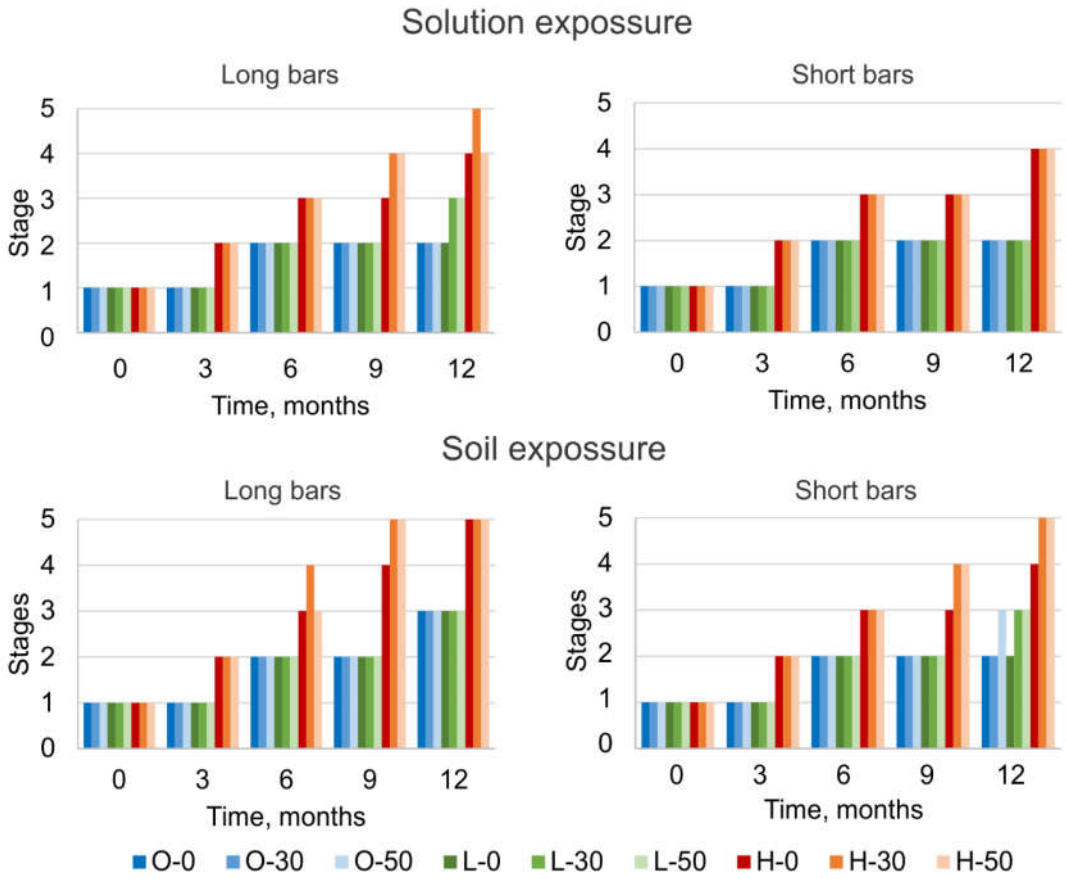

Figure 6 – Deterioration stages by visual inspection, up to 12 months.

In qualitative terms, it was observed a slight difference in the deterioration mechanisms of specimens regarding the exposure type. Solution-exposed bars showed progression a bit more uniform than soil-exposed bars. On the one hand, exposure to sulfate solution is based mainly on diffusion, which is uniform throughout the whole bar. The cracking development was uniform as described by the stages, and a high bending of the shaft was observed in all samples before failure. On the other hand, in the soil-exposed specimens, there is also a sulfate ingress with water transport. This mechanism is more sensitive to local defects (big pores, mesocracking, etc.). In this case, the cracking development was more concentrated in spots, and the failure of specimens was earlier than shaft bending in most of cases

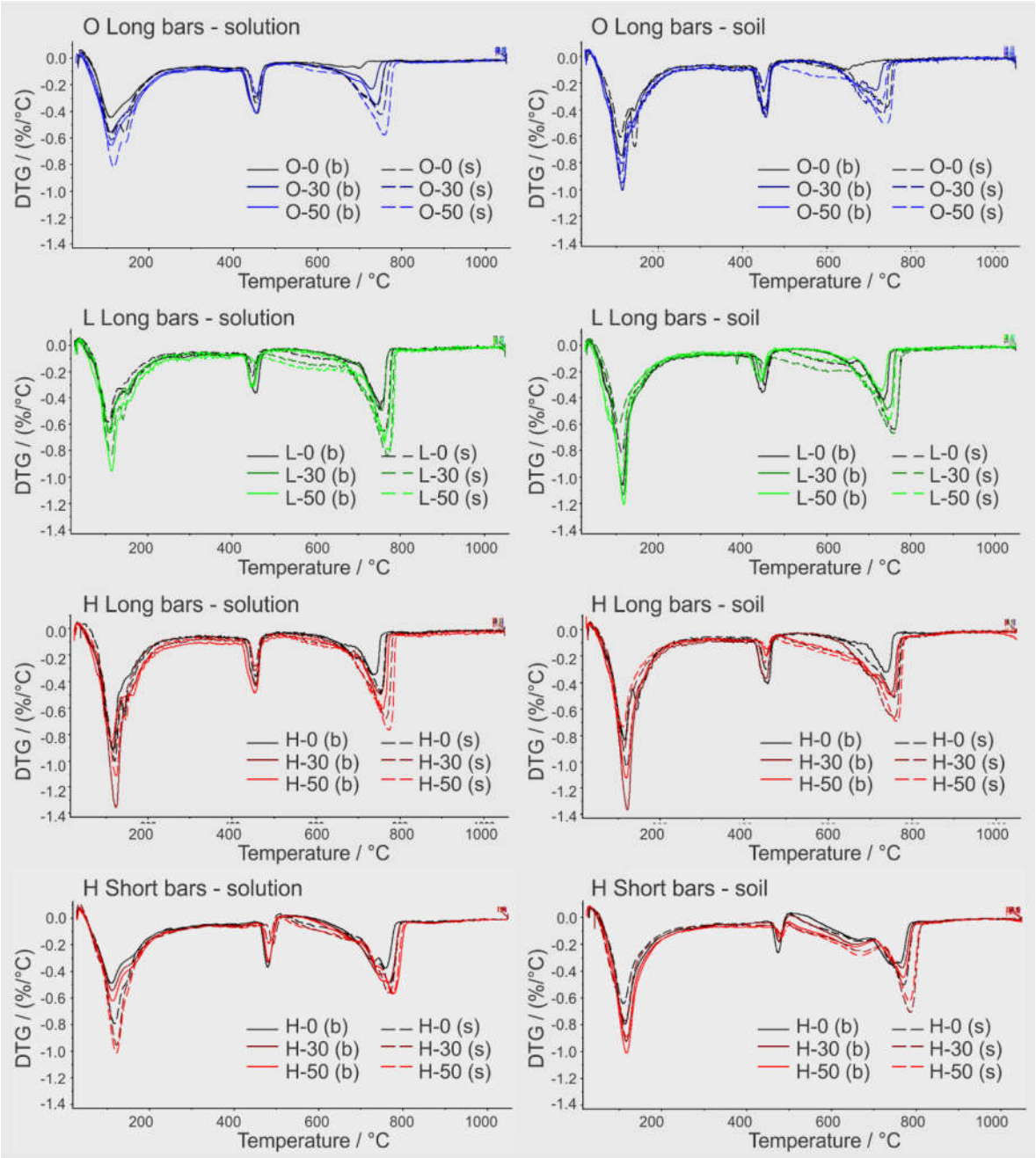

Figure 7 – DTG curves of mortars after 1 year of exposure

4. MICROSTRUCTURAL ANALYSIS

4.1. Thermogravimetric analyses

Figure 7 shows the DTG curves for all samples analyzed. Although all samples showed similar peak distributions (characteristic peaks described in the Methodology section), some differences are observed owing to the location of the sample (bulk or surface), as well as the FRA content or the cement type of the mortars.

In general terms, surface samples showed lower contents of portlandite with respect to bulk samples. Moreover, all mortars showed a higher content of carbonates at the surface than in the bulk. Both phenomena are attributed to the carbonation of samples during preparation and the exposure of samples, which has a gradient from the surface to the bulk. The same is observed for long bars exposed to sulfate soil, with slight differences on the carbonates' peak shapes. In both portlandite and carbonates peaks, there is also a visible effect of FRA content. The higher the FRA content, the larger the carbonate peak. However, it should be kept in mind that initial carbonate content might be affected by FRA content as it contains attached (probably carbonated) cement paste (continue in Section 4.1.1).

Regarding the range of 50-200 °C, there are clear differences regarding the cement type. For long bars exposed to solution, H mortars showed bigger peaks than L and O mortars, even in bulk samples. Bigger peaks in this range are observed for series exposed to sulfate soil, which evidences a higher extent of deterioration for ESA in combination with PSA. H-mortar short bars showed smaller peaks than long bars in this range, especially in bulk samples. This is attributed to the size effect on the ESA kinetics.

4.1.1. Solution-exposed samples

Results of mineral quantifications (calculated as mentioned in section 2.4) for solution-exposed samples are presented in Figure 8. In general, mineral contents differed consistently between bulk and surface samples, consistent with the mechanisms of ESA that start at the surface and progress in the bulk. It was also observed an effect of the cement type and the FRA content in mixes. When comparing the last two groups (long and short bars of the H series), some differences linked to the slenderness of specimens are also observed. Relative amounts of cement phases are presented relative to the total weight of the samples. These values are comparable to mineral quantifications of cement-based materials affected by ESA reported in the literature [33,53].

In terms of ESA products, there was a slightly higher presence of ettringite and gypsum observed in the H mortars compared to the O and L series. Additionally, the H-30 mortar, which had exhibited the highest level of macroscopic deterioration, showed also a greater amount of ettringite in its bulk sample. It's important to note that the total quantity of ESA products does not necessarily correlate with the extent of deterioration, since damage occurs when the material's buffer capacity is depleted [33,53], and according to the crystallization pressure hypothesis, only ettringite present in small micropores is responsible for initiating cracking. However, in this case, the non-linear impact of FRA content on ESA progression was also observed in thermogravimetric quantification. The positive effect of a higher buffer capacity and the negative effect of a higher transport rate, make ambiguous the effect of the FRA content.

Ettringite contents are always higher in surface samples than in bulk samples (except in H-30 mortar), and the same occurs with gypsum. As sulfate ions come in from the surface, both minerals are found in greater quantities in surface samples. Higher contents of gypsum were observed on the surface than in the bulk for almost all series. Because the amounts of gypsum determined are quite small, the quantification accuracy might be lower (near the detection limit of the method). For H-series short bars, the content of ettringite in bulk samples is lower than that in long bars, and even similar to that in O mortars. However, higher contents of ettringite are observed in surface samples. This evidences a different mechanism of deterioration by ESA depending on specimen size and shape.

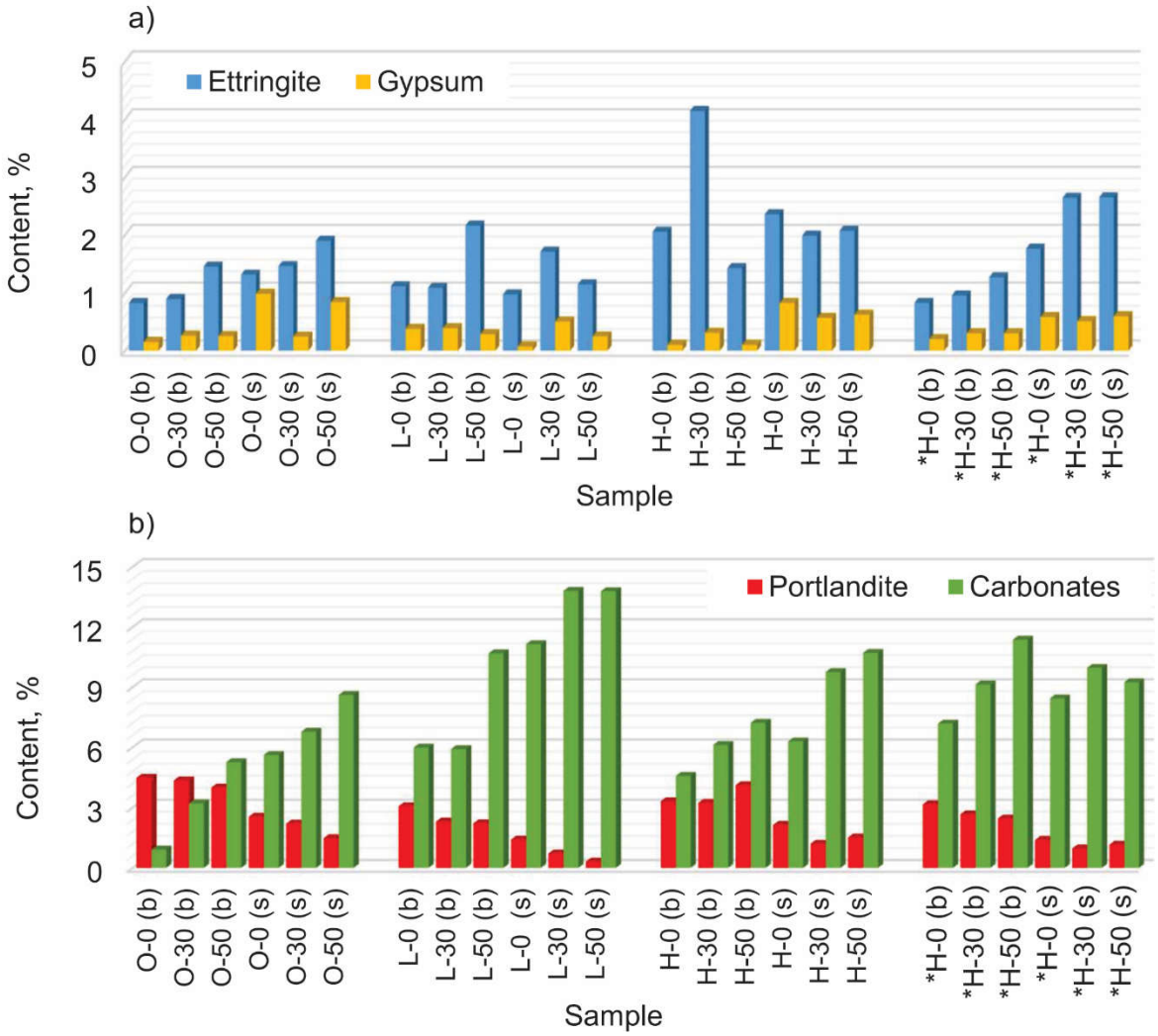

Figure 8 – Mineral quantification in mortar bars exposed to sulfate solution for up to 12 months: a) ESA products; b) common cement paste minerals.
(Mixes nomenclature: b=bulk samples; s=surface samples, *=short bars)

The reduction of portlandite amounts in samples is related to the degree of carbonation, which consumes it to form calcite, and to the development of ESA, which consumes it to form gypsum and ettringite. In all samples, more portlandite was found in the bulk than in the surface samples. Then, for all groups, a higher portlandite loss is observed when FRA content

increases. The only exception to this is for H mortar long bars. In this case, the lowest portlandite content corresponds with H-30 mortar (higher ettringite+gypsum content and higher expansion). Initial contents of carbonates are linked with the cement type of the mortar (limestone filler) and can be affected by the attached mortar of FRA. Assuming that all attached mortar of FRA was carbonated before used, the maximum increase in total carbonate content could be up to approximately 2 and 4% for 30 and 50% FRA content, respectively. Then, results showed higher increments of carbonate contents in samples when FRA content increased; hence, the higher porosity of mortars with FRA might have accelerated the carbonation progression.

4.1.2. Soil-exposed samples

Results of mineral quantifications for soil exposure samples are presented in Figure 9. As in solution-exposed samples, there are clear differences between bulk and surface samples, which are related to the deterioration mechanism. Then, there are observed differences regarding the cement type and FRA content of mortars, and the slenderness of specimens. Moreover, the PSA action might increase the permeability of specimens to aggressive agents, changing the combined mechanism of deterioration.

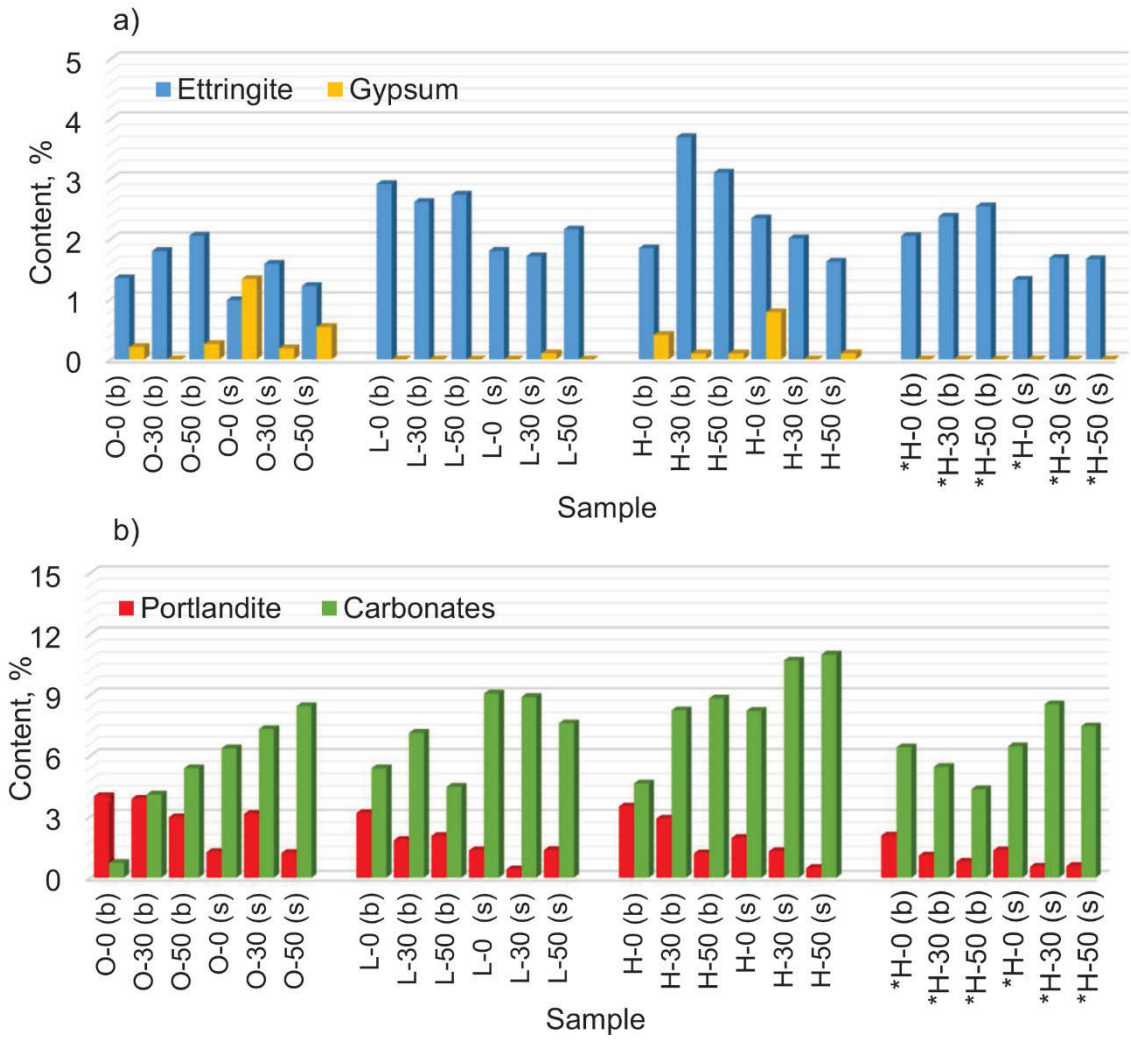

Figure 9 – Mineral quantification in mortar bars exposed to sulfate soil for up to 12 months: a) ESA products; b) common cement paste minerals.
(Mixes nomenclature: b= bulk samples; s= surface samples, *= short bars)

In contrast with solution-exposed samples, higher contents of ettringite are observed in bulk samples than in surface samples, in general. In this case, the PSA mechanism accelerates the ion ingress to the whole sample, and later, it seems that ESA post-mortem products were more stable in bulk samples than in surface samples. Furthermore, the effect of the cement type is not as visible as in the solution-exposed series. For instance, the L series seems to show similar ettringite contents to the H series. It should be noted that H mortars had suffered a severe degradation at the moment of sample extraction, whereas L specimens had shown small and isolated cracks, similar to the O series. This may allow a loss of post-mortem ESA products during the manipulation of the specimens (they were washed after each measurement) and samples extraction.

For example, the control mortar of the L series showed a higher ettringite content than the H control mortar, but the latter showed a gypsum content, which is a post-mortem ettringite remainder. Also, gypsum was detected in surface samples of O mortars, which had a higher relative content of portlandite than limestone filler types of cement (L and H).

Regarding the FRA content, the ettringite amount showed different trends according to the cement type. For the O series bulk samples, a higher ettringite content is observed as FRA content increases, but for surface samples, a higher content is observed for 30% FRA mortar. For L series, no significant variations due to FRA contents are observed.

For the H series, mortars with FRA showed more ettringite content in the bulk than the control mortar. However, surface samples showed lower contents of ettringite as FRA content increased. This is showing that considerable amounts of ettringite could have precipitated as gypsum in an advanced stage of attack, and then some of the latter was lost during the sample extraction and preparation processes.

Portlandite contents showed, in general, a reduction when FRA content increased, and, secondarily, a reduction in surface samples compared to bulk samples. Both phenomena are related with the ESA and carbonation mechanisms. Results suggest that the higher porosity of FRA increased the kinetics of both phenomena. However, there are some samples that do not comply with the general trend. For the O series, a clear relationship is observed between the portlandite reduction and gypsum observed in surface samples. For the L series, a lower portlandite content is observed in the mortar with 30% FRA.

Regarding the carbonates, there are in general higher contents in the surface samples than in those from the bulk, but variable effects of the FRA content for each series. For O and H, long bar series, the carbonate content was quite proportional to the FRA content. Conversely, for L mortars, the general correlation was in the opposite direction, as in the bulk samples of H-mortar short bars. Then, higher amounts of carbonates were found in mortars with 30% FRA. Thereby, it seems that the more heterogeneous cracking mechanism of the ESA+PSA exposure condition might induce difficulties in the sample extraction and its representativeness at this scale of analysis.

The earliest damage observed in H mortars is likely related to higher ettringite formation due to the high C_3A content in the cement. It is possible that a certain amount of ettringite

decomposes when porosity suddenly increases and thermodynamic conditions change due to cracking. Normally, ettringite decomposes to gypsum when the pH decreases or the sulfate concentration is high [36,54,55]. Thereafter, it is possible that limestone cements form monocarbonate, which is a more stable phase than gypsum [55] and whose peak is near the range of gypsum and ettringite. This could result in an overestimation of ettringite contents in L mortars, for instance.

4.2. Microscopic analyses

Microscopic and compositional analyses were performed using SEM/EDX instruments. Microscopic inspection was done on samples taken from the same specimens as for thermogravimetric analyses. Analysis included general characterization of cracking, examination of ESA-related compounds, and interaction of FRA with attack progression (analysis of surface and bulk zones of specimens).

4.2.1. Solution-exposed samples

Microscopic inspections revealed signs of ESA due to the presence of ettringite and gypsum in all samples, even in the mortar samples with low-C_3A cement. Also, different levels of cracking were observed in mortar samples. Special attention was given to RCA particles and their surroundings, in order to know their participation in the ESA process.

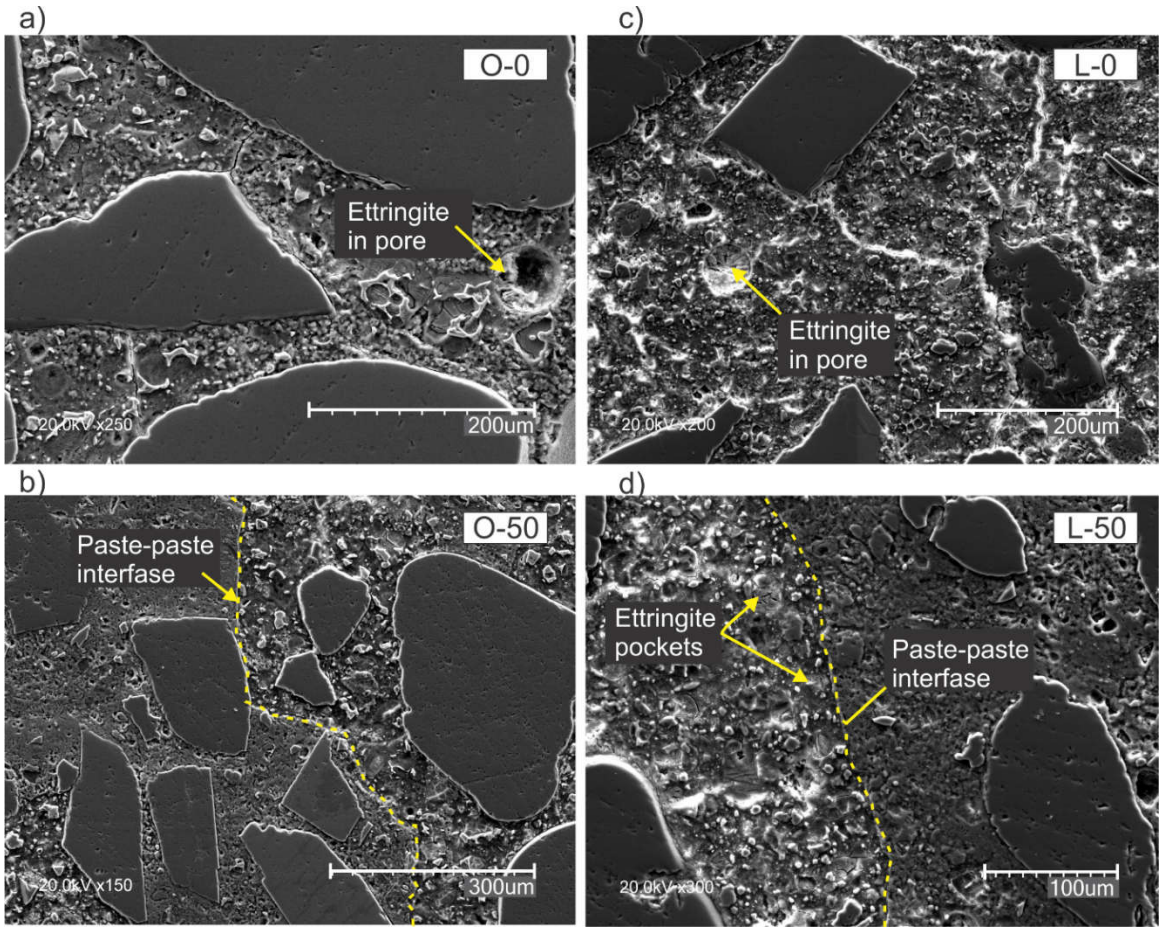

Figure 10 – SEM/BSE images of O and L mortar specimens after 1 year to sulfate-solution exposure: a) O-0 sample; b) O-50 sample; c) L-0 sample; d) L-50 sample.

For samples of O and L mortars, some isolated microcracking (<5um) was observed (Figure 10). However, since they were empty of ESA products in general, it is possible that they are related to cracks induced in the sample extraction. In all samples, several small pores (between 30 and 200 µm) were observed fully or partially filled with ettringite. These entrapped-air voids could act as a buffer for the mortars [33,56], altering the relationship between the ESA mass changes and the rate of deterioration. As the use of FRA could increase air incorporation [32,57], this could result in a positive effect of its use. Furthermore, ettringite was detected in small pockets within the cement matrix, associated with production of non-connected cracking.

In the case of H mortar samples, the development of cracking was greater than in the O and L series. The small pores of entrapped air were in general filled with ESA products, indicating a consumption of the buffer capacity, and pockets of ettringite in the cement matrix were observed with associated cracking. Moreover, for this series, a larger development of cracking was observed, generally filled with ESA products (Figure 11). This is consistent with macroproperties observed, where H mortars exhibited the highest deterioration values.

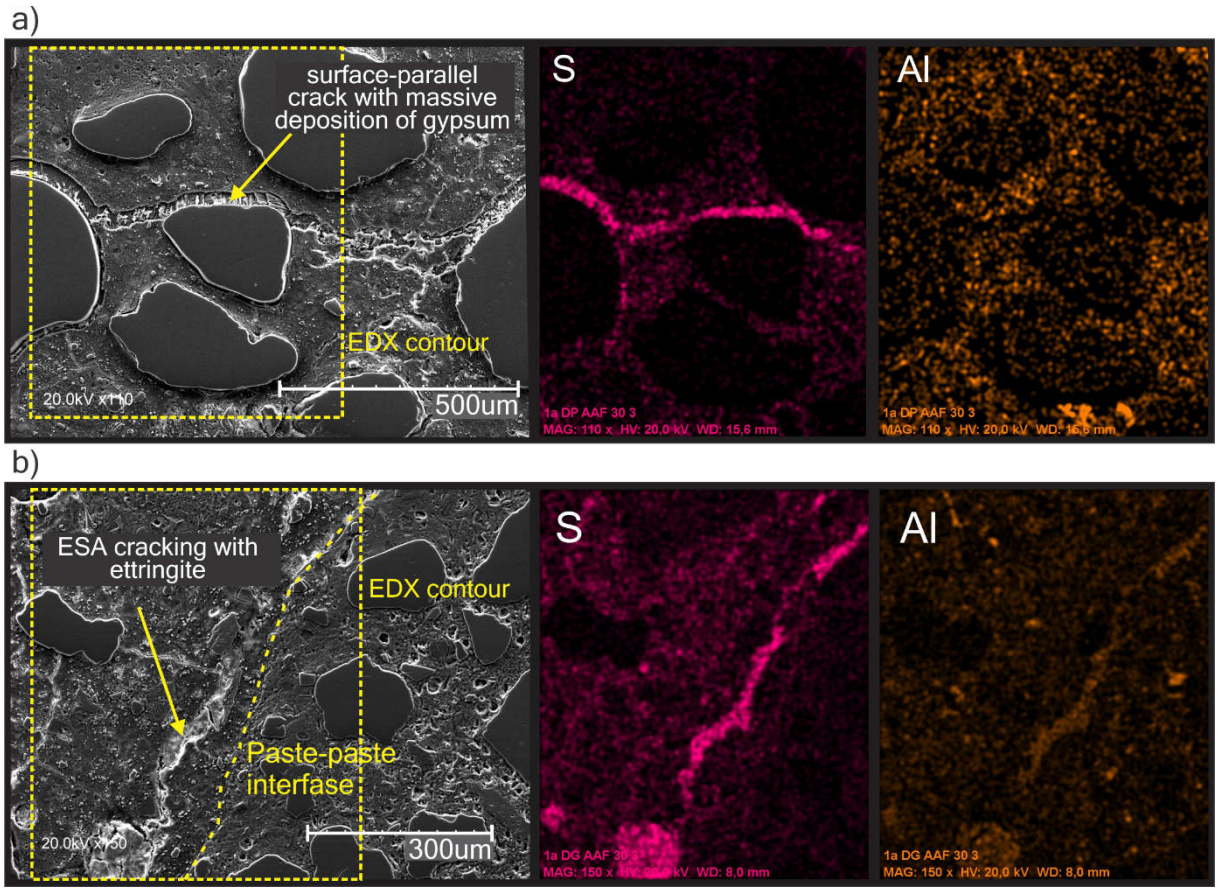

Figure 11 – SEM/BSE images and corresponding EDX mappings of sulfur (S) and aluminum (Ai); a) Near-surface region of an H-30 long bar; b) Bulk region of an H-30 short bar.

The image in Figure 11a was taken near the surface region of an H-30 long bar sample. A crack of approximately 30 µm, filled, parallel to the surface, is observed, which opens through

the interfacial transition zone and the cement paste matrix. The EDX analysis confirms that the filling material in the cracks corresponds mainly to gypsum (high sulfate concentration and no aluminum). These types of filled cracks are post-mortem evidence of ESA propagation. The higher crack formation near the surface allows the sulfate concentration to increase, and gypsum becomes more stable than ettringite.

The image in Figure 11b was taken from the bulk region of an H-30 short bar sample. In this case, the wider cracks related to ESA progression appear filled with ettringite since EDX mappings showed a higher sulfur and aluminum concentration in there. In the same image, an interface between the old mortar attached to an FRA particle and the new cement matrix is observed. There, the ESA crack connects a part of the paste-paste interface with a pore of the cement matrix fully filled with ettringite. This distribution of ettringite and gypsum in the bulk and the surface, respectively, was generally observed, supporting the hypothesis that ettringite is more associated with the formation of cracks (front of attack), and the presence of massive gypsum serves as post-mortem evidence in larger cracks [34,58].

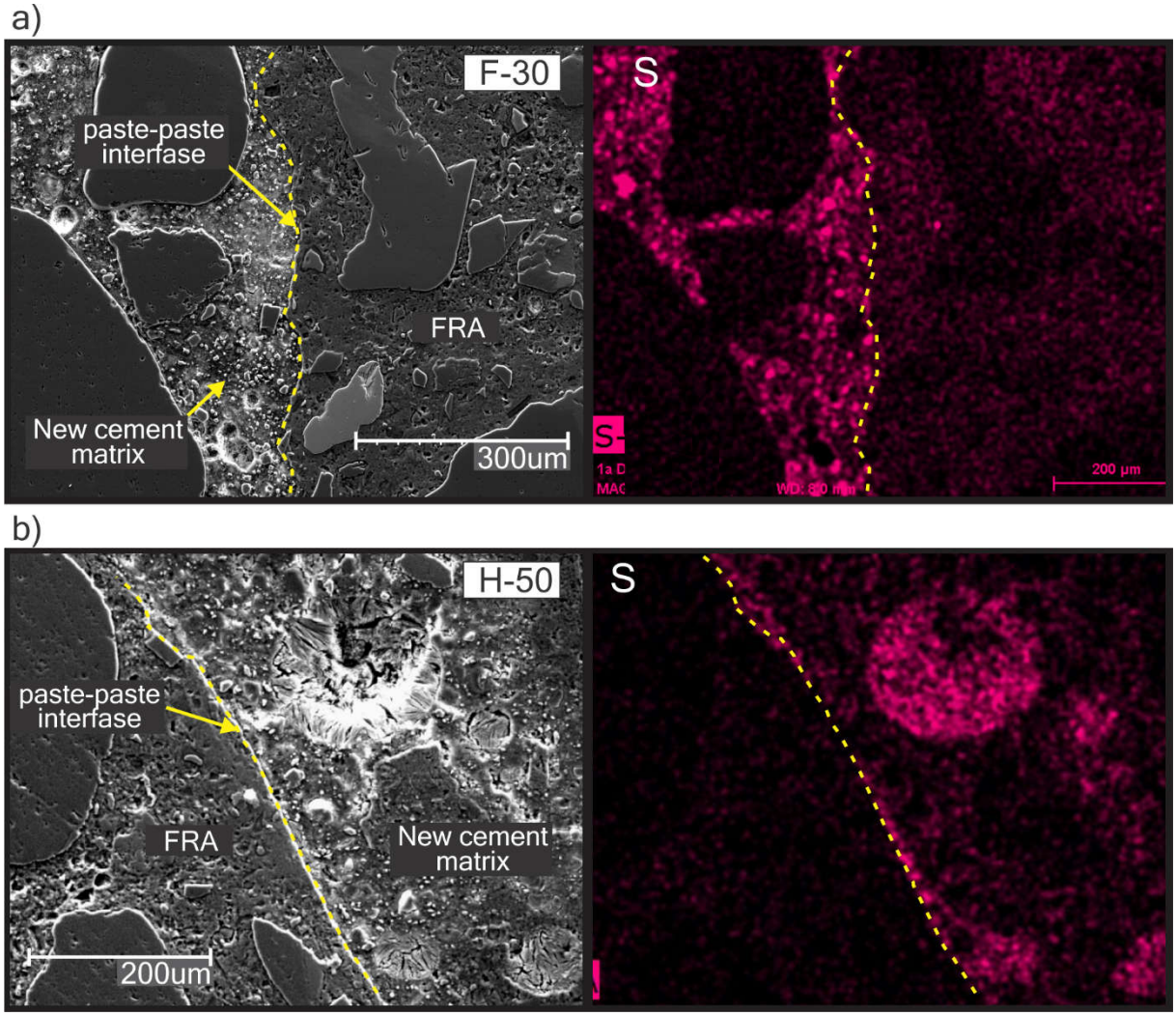

Figure 12 – SEM/BSE-EDX mappings of sulfur (S) images of interfacial transition zone between a FRA particles and the new matrix of mortar, of samples exposed to sulfate solution. a) L-30 mortar sample; b) H-50 mortar sample.

Regarding the FRA inspection, it was generally observed that the attached cement paste had a lower sulfate content than the new cement matrix. Figure 12 shows two examples of the interfacial transition zone between a FRA particle and the cement matrix of the mortar (new and old cement paste). The upper image corresponds to a low C_3A cement mortar (L-30), and the lower image corresponds to a high C_3A cement mortar (H-50). In both cases, a higher concentration of sulfates in the new cement matrix than in the old attached cement paste is observed. This could indicate two possibilities: that the sulfate ions penetrate the FRA particles in lower amounts (incoherent porosity) or that the ions penetrated the FRA particles but did not found binding minerals to react with and precipitate (reduced AFm and/or portlandite content). It should be kept in mind that FRA cement paste probably has a high degree of carbonation, which means a lower content of portlandite, from which gypsum and then ettringite are formed. The microcracks associated with the precipitation of ESA products almost always occurred in the new cement matrix and not in the old cement paste. This situation was observed in all samples exposed to sulfate solution and confirmed by EDX point analyses.

4.2.2. Soil-exposed samples

Samples exposed to sulfate-rich soil were found to develop a greater extent and width of crack compared to solution-exposed samples. This is attributed to the physical action of salt crystallization in combination with ESA.

In contrast with solution-exposed samples, in O and L samples, a small (< 5 μm) but more notorious mapping-arrangement cracking was observed, especially near the surface. Figure 13 shows examples of this cracking development. The elemental composition did not show ESA products on these cracks, and this suggests that this cracking is due to the physical action of salt crystallization. They also could be formed by the samples' extraction, but the good state of these mortars bars reduces this possibility. As was observed in solution-exposed samples, it is observed that pores are fully or partially filled with ettringite.

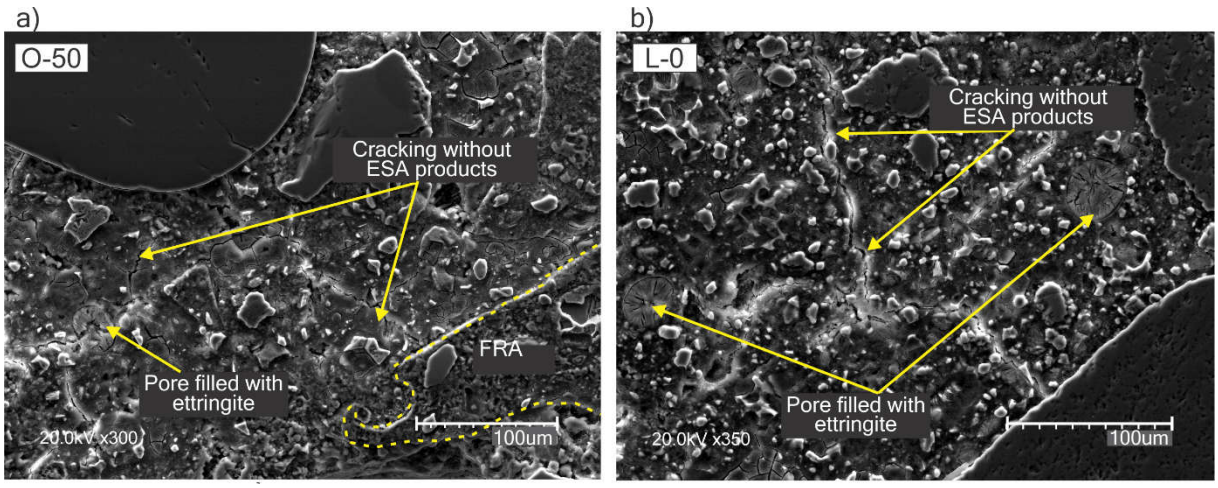

Figure 13 – SEM/BSE images of O and L mortar specimens after 1 year to sulfate-soil exposure: a) O-50 sample; b) L-0 sample.

For H mortars the cracking development was greater, and also a larger-scale cracking is observed. In Figure 14, some examples of these cracks are presented. Cracks with even 100 μm width are observed throughout the section, around natural aggregate interfaces and

cement matrix. A characteristic of these cracks is that they do not run parallel to the surface as pure ESA cracks do. In some cases, they run perpendicular to the surface and penetrate the sample with a pattern arrangement. Also, lower-scale microcracking is observed on the cement matrix, with ESA products filling cracks or in small pockets.

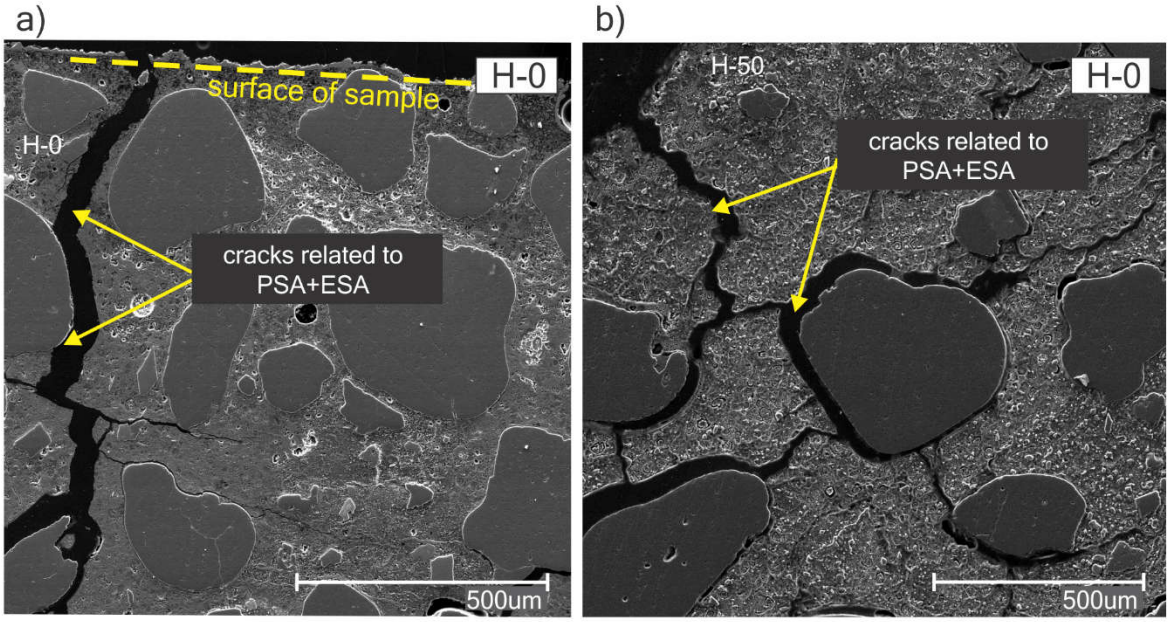

Figure 14 –SEM/BSE images of specimen exposed to sulfate-rich soil up to 12 months: a) Near surface region of H-0 mortar sample; b) Bulk region of H-0 mortar sample.

As was observed in samples exposed to sulfate solution, the sulfur mapping showed lower binding of sulfate ions in the old cement paste attached to FRA particles (Figure 15). In general, the attached cement paste from FRA showed a lower microcracking development than the new cement matrix. However, it can be observed that some cracking development is coherent between the matrix and FRA particles, as in the example presented in Figure 15. Also in this case, the sulfur content in FRA paste is lower than in cement matrix.

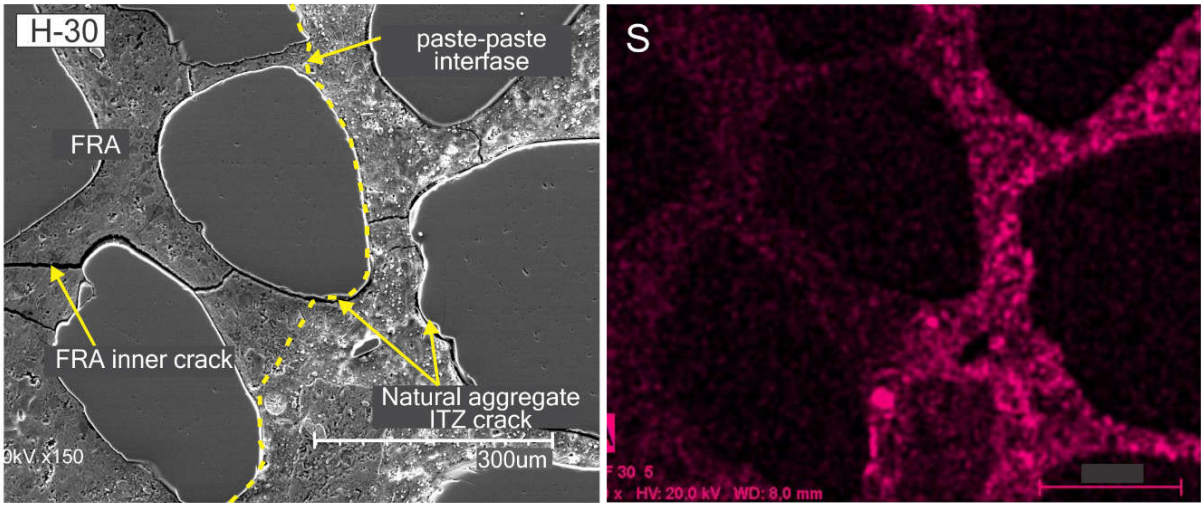

Figure 15 - SEM/BSE-EDX images of interfacial transition zone between an FRA particles and the new matrix of mortar H-30, exposed to sulfate soil.

5. DISCUSION

The results of these experiences shed light on the role of recycled aggregate particles in terms of sulfate attack and associated degradation processes (PSA and carbonation). The evaluation of macro-properties has shown that mortars with low alumina cement maintain their sulfate resistance even in mortars with 50% FRA content. In this case, the aluminum content of the source concrete from which the FRA was obtained is unknown, but it can be expected that it was made with a low-C_3A cement, since Argentinian cement has a low content of this phase in general. When mortars were exposed to unsaturated conditions and PSA could develop, the higher porosity of mortars with FRA appears to have had a negative effect, even when using advantageous cement. Mortars with O and L cements (4.9 and 3.2% C_3A content, respectively) showed different behavior depending on the FRA content, but differences were not significant.

An FRA effect on mortars behavior was observed in the high C_3A cement used (H series mortar)). Particularly in the case of solution-exposed samples, the mortars with 30% FRA showed worse performance than the control mortars and the mortars with 50% FRA. Although a high porosity of mortar (or concrete) is considered to enhance ESA kinetics and expansion, porosity affects through multiple mechanisms other than just increasing the sulfate penetration rate [33]. The porosity corresponding to the entrapped air may act as a buffer against the ESA products precipitation. The higher porosity of FRA also results in a lower stiffness of whole material, which can contribute to a reduction in the internal restraint of the specimen and less internal stresses [59], and consequently less cracking.

Microstructural inspection showed no significant precipitation of external sulfate ions in FRA particles, and almost no cracking associated with the precipitation of ettringite or gypsum was observed. This finding supports the hypothesis of the reduction of internal restriction, i.e., the contribution of FRA deformability for a better behavior against expansion due to ESA. The combination of factors affecting internal restriction and ESA kinetics (e.g., specimen shape, type, and degree of exposure, cement matrix) appears to modify the optimum FRA content regarding the resistance in this exposure.

An increase in FRA content leads to an increase in the overall porosity of the mortar, but the net effect depends on whether the predominant influence is on the sulfate penetration rate, the development of internal stresses, or the degree of internal confinement. This ambiguous effect of recycled aggregate content on specimen deterioration has also been observed in other studies in the literature [27,60,61], but further research is necessary for a comprehensive understanding of this phenomenon. It should also be noted that, in this case, only one cement with high C_3A was evaluated, and the effect of RCA in mixes with other cement types (e.g., different C_3A content, different C_3S/C_2S ratio, MCS) could vary.

A few other experiences in the literature showed that mortars or concretes containing recycled aggregates had lower expansion or damage than control mixes, in agreement with the results of the present study. For example, Lee et al [24] studied mortar mixes with 0, 25, 50, 75, and 100% FRA exposed to a sulfate solution. They reported lower expansion of 25 and 50% FRA mixes and higher expansion of 75 and 100% mixes, compared to control mortar. Boudali et al [31] reported a smaller decrease in strength and mass loss in SCC with recycled aggregates compared to control mixes. Santillán et al [27] observed similar or even superior behavior in

concretes with coarse recycled aggregates compared to control concretes when subjected to long-term exposure to sulfate solution. Candamano et al [59] reported a lower loss in compressive strength of mortars with 100% of FRA in thixotropic mortars. The contribution of recycled aggregates to reduce internal restriction can provide a plausible hypothesis to explain all these results.

6. CONCLUSIONS

In this paper, multiple instrumental analyses were applied to describe the effects of FRA content on mortar exposed to different types of sulfate environments. Macro properties such as expansion, weight change, and visual inspections were performed after 12 months of exposure. The microstructure of samples was analyzed by thermogravimetric analysis and microscopic X-ray examination. The following outcomes are stated:

- Macroscopic and microstructural studies confirmed that the effect of the FRA content on the behavior of mortar against sulfate attack is not linear with its replacement percentage. Although a higher permeability to sulfate penetration is attributed to the higher porosity of the FRA mortars, a positive effect can be attributed to a lower internal restriction against ESA expansion. The relation between the two opposite effects seems to have an optimum value that depends on other test parameters. In this case, the worse behavior corresponds to a replacement of 30% for FRA.
- In the saturated state, FRA content affects the behavior of cement mortars against sulfate only when the cement matrix has a poor chemical quality (i.e., a high C_3A content). In the unsaturated state, cement-based mortars with low C_3A content showed a slight effect of the FRA content.
- The exposure to sulfate-soil showed a higher rate of degradation in samples than solution exposure. This is due to the combined effect of PSA with pure ESA.
- The size and shape of specimens had an impact on the kinetics of degradation, in both solution and soil exposure type.
- Microscopic analysis showed a lower binding of sulfate ions in the cement paste attached to FRA particles. This can be related to a good quality in the interface (disconnected porosity) or to a lower binding capacity of the old cement paste (lower available portlandite or aluminate phases).
- The optimal combination of positive and negative effects of FRA is influenced by other parameters of the test setup, such as the size and shape of the specimens, the type of exposure, and the properties of the cement matrix. Further research may confirm whether this phenomenon also affects concrete specimens with coarse recycled aggregate, causing a different relationship between the internal restriction and ESA progression.

Acknowledgements

The financial support from the National Agency for the Promotion of Research, Technological Development and Innovation (Agencia I+D+i) through Fund for Scientific and Technological Research (FONCYT), PICT 2015-3339 and PICT 2017-0091 Prest BID, for this publication is greatly appreciated.

References

[1] K.P. Mehta, Reducing the environmental impact of concrete, Concr. Int. 23 (2001) 61–

66. https://www.concrete.org/publications/internationalconcreteabstractsportal.aspx?m=details&ID=10735 (accessed February 3, 2019).

[2] A. Abbas, G. Fathifazl, O.B. Isgor, A.G. Razaqpur, B. Fournier, S. Foo, Environmental benefits of green concrete, in: EIC Clim. Chang. Technol. Conf. 10-12 May 2006, Otawa, Canada, IEEE, 2006.

[3] T.C. Hansen, Recycled aggregates and recycled aggregate concrete second state-of-the-art report developments 1945-1985, Matériaux Constr. 19 (1986) 201–246.

[4] A. Akhtar, A.K. Sarmah, Construction and demolition waste generation and properties of recycled aggregate concrete: A global perspective, J. Clean. Prod. 186 (2018) 262–281. https://doi.org/10.1016/j.jclepro.2018.03.085.

[5] R.K. Dhir, M.C. Limbachiya, T. Leelawat, Suitability of Recycled Concrete Aggregate for Use in Bs 5328 Designated Mixes., Proc. Inst. Civ. Eng. - Struct. Build. 134 (1999) 257–274. https://doi.org/10.1680/istbu.1999.31568.

[6] K.A. Paine, R.K. Dhir, Recycled aggregates in concrete: A performance-related approach, Mag. Concr. Res. 62 (2010) 519–530. https://doi.org/10.1680/macr.2010.62.7.519.

[7] Rasheeduzzafar, A. Khan, Recycled Concrete—A Source for New Aggregate, Cem. Concr. Aggregates. 6 (1984) 17–27. https://doi.org/10.1520/CCA10349J.

[8] A.K. Padmini, K. Ramamurthy, M.S. Mathews, Influence of parent concrete on the properties of recycled aggregate concrete, Constr. Build. Mater. 23 (2009) 829–836. https://doi.org/10.1016/j.conbuildmat.2008.03.006.

[9] C.J. Zega, Propiedades Físico - Mecánicas y Durables de Hormigones Reciclados, Universidad Nacional de La Plata, 2010.

[10] B. González-Fonteboa, S. Seara-Paz, J. De Brito, I. González-Taboada, F. Martínez-Abella, R. Vasco-Silva, Recycled concrete with coarse recycled aggregate. An overview and analysis, Mater. Constr. 68 (2018) 1–29. https://doi.org/10.3989/mc.2018.13317.

[11] S.W. Tabsh, A.S. Abdelfatah, Influence of recycled concrete aggregates on strength properties of concrete, Constr. Build. Mater. 23 (2009) 1163–1167. https://doi.org/10.1016/j.conbuildmat.2008.06.007.

[12] J.M. Gómez-Soberón, Porosity of recycled concrete with substitution of recycled concrete aggregate. An experimental study, Cem. Concr. Compos. 32 (2002) 1301–1311. https://doi.org/10.1016/s0008-8846(02)00795-0.

[13] C.S. Poon, Z.H. Shui, L. Lam, Effect of microstructure of ITZ on compressive strength of concrete prepared with recycled aggregates, Constr. Build. Mater. 18 (2004) 461–468. https://doi.org/10.1016/j.conbuildmat.2004.03.005.

[14] C.J. Zega, Á.A. Di Maio, R. Zerbino, Influence of Natural Coarse Aggregate Type on the Transport Properties of Recycled Concrete, J. Mater. Civ. Eng. 26 (2014).

[15] A. Gonçalves, A. Esteves, M. Vieira, Influence of recycled concrete aggregates on concrete durability, in: E. Vázquez, C.F. Hendriks, G.M.T. Janssen (Eds.), Int. RILEM Conf. "The Use Recycl. Mater. Build. Struct., Barcelona, Spain, 2004: pp. 554–562.

[16] E. Vázquez, Recycled Concrete, in: 2013: pp. 175–194. https://doi.org/10.1007/978-94-007-4908-5_4.

[17] C. Thomas, J. Setién, J.A. Polanco, P. Alaejos, M. Sánchez De Juan, Durability of recycled aggregate concrete, Constr. Build. Mater. 40 (2013) 1054–1065. https://doi.org/10.1016/j.conbuildmat.2012.11.106.

[18] J. De Brito, J. Ferreira, J. Pacheco, D. Soares, M. Guerreiro, Structural, material, mechanical and durability properties and behaviour of recycled aggregates concrete, J. Build. Eng. 6 (2016) 1–16. https://doi.org/10.1016/j.jobe.2016.02.003.

[19] C.J. Zega, L.R. Santillán, M.E. Sosa, Y.A. Villagrán Zaccardi, Durable Performance of

Recycled Aggregate Concrete in Aggressive Environments, J. Mater. Civ. Eng. 32 (2020) 1–10. https://doi.org/10.1061/(ASCE)MT.1943-5533.0003253.

[20] H. Guo, C. Shi, X. Guan, J. Zhu, Y. Ding, T.C. Ling, H. Zhang, Y. Wang, Durability of recycled aggregate concrete – A review, Cem. Concr. Compos. 89 (2018) 251–259. https://doi.org/10.1016/j.cemconcomp.2018.03.008.

[21] R. Somna, C. Jaturapitakkul, A.M. Amde, Effect of ground fly ash and ground bagasse ash on the durability of recycled aggregate concrete, Cem. Concr. Compos. 34 (2012) 848–854. https://doi.org/10.1016/j.cemconcomp.2012.03.003.

[22] V. Bulatovic, M. Melesev, Evaluation of sulfate resistance of concrete with recycled and natural aggregates, Constr. Build. Mater. 152 (2017) 614–631. https://doi.org/10.1016/j.conbuildmat.2017.06.161.

[23] S. Boudali, A.M. Soliman, B. Abdulsalam, K. Ayed, D.E. Kerdal, S. Poncet, A. Materials, Microstructural Properties of the Interfacial Transition Zone and Strength Development of Concrete Incorporating Recycled Concrete Aggregate, Int. J. Struct. Constr. Eng. 11 (2017) 1012–1016.

[24] S. Lee, R.N. Swamy, S. Kim, Y. Park, Durability of Mortars Made with Recycled Fine Aggregates Exposed to Sulfate Solutions, J. Mater. Civ. Eng. 20 (2008) 63–70.

[25] C.J. Zega, G.S. Coelho Do Santos, Y.A. Villagrán Zaccardi, A.A. Di Maio, Performance of recycled concretes exposed to sulphate soil for 10 years, Constr. Build. Mater. 102 (2016) 714–721. https://doi.org/10.1016/j.conbuildmat.2015.11.025.

[26] C. Colman, D. Bulteel, V. Thiery, S. Rémond, F. Michel, L. Courard, Internal sulfate attack in mortars containing contaminated fine recycled concrete aggregates, Constr. Build. Mater. 272 (2021) 121851. https://doi.org/10.1016/j.conbuildmat.2020.121851.

[27] L.R. Santillán, F. Locati, Y.A. Villagrán-Zaccardi, C.J. Zega, Long-term sulfate attack on recycled aggregate concrete immersed in sodium sulfate solution for 10 years, Mater. Constr. 70 (2020) 1–14. https://doi.org/10.3989/mc.2020.06319.

[28] A. Yammine, M. Hamdadou, N. Leklou, F. Bignonnet, M. Choinska-colombel, Effect of recycled concrete aggregates and recycled filler on delayed ettringite formation : An experimental study compared to chemical modelling, Cem. Concr. Compos. 132 (2022) 104636. https://doi.org/10.1016/j.cemconcomp.2022.104636.

[29] P. Rattanachu, W. Tangchirapat, C. Jaturapitakkul, Water Permeability and Sulfate Resistance of Eco-Friendly High-Strength Concrete Composed of Ground Bagasse Ash and Recycled Concrete Aggregate, J. Mater. Civ. Eng. 31 (2019). https://doi.org/10.1061/(ASCE)MT.1943-5533.0002740.

[30] H. Zhang, T. Ji, H. Liu, Performance evolution of recycled aggregate concrete (RAC) exposed to external sulfate attacks under full-soaking and dry-wet cycling conditions, Constr. Build. Mater. 248 (2020) 118675. https://doi.org/10.1016/j.conbuildmat.2020.118675.

[31] S. Boudali, D.E. Kerdal, K. Ayed, B. Abdulsalam, A.M. Soliman, Performance of self-compacting concrete incorporating recycled concrete fines and aggregate exposed to sulphate attack, Constr. Build. Mater. 124 (2016) 705–713. https://doi.org/https://doi.org/10.1016/j.conbuildmat.2016.06.058.

[32] A. Yammine, N. Leklou, M. Choinska, F. Bignonnet, J. Mechling, DEF damage in heat cured mortars made of recycled concrete sand aggregate, Constr. Build. Mater. 252 (2020) 119059. https://doi.org/10.1016/j.conbuildmat.2020.119059.

[33] T. Ikumi, S.H.P. Cavalaro, I. Segura, The role of porosity in external sulphate attack, Cem. Concr. Compos. 97 (2019) 1–12. https://doi.org/10.1016/j.cemconcomp.2018.12.016.

[34] W. Kunther, B. Lothenbach, K.L. Scrivener, On the relevance of volume increase for the length changes of mortar bars in sulfate solutions, Cem. Concr. Res. 46 (2013) 23–29.

https://doi.org/10.1016/j.cemconres.2013.01.002.
[35] X. Brunetaud, M.R. Khelifa, M. Al-Mukhtar, Size effect of concrete samples on the kinetics of external sulfate attack, Cem. Concr. Compos. 34 (2012) 370–376. https://doi.org/10.1016/j.cemconcomp.2011.08.014.
[36] T. Schmidt, B. Lothenbach, M. Romer, J. Neuenschwander, K. Scrivener, Physical and microstructural aspects of sulfate attack on ordinary and limestone blended Portland cements, Cem. Concr. Res. 39 (2009) 1111–1121. https://doi.org/10.1016/j.cemconres.2009.08.005.
[37] P. Feng, E.J. Garboczi, C. Miao, J.W. Bullard, Microstructural origins of cement paste degradation by external sulfate attack, Constr. Build. Mater. 96 (2015) 391–403. https://doi.org/10.1016/j.conbuildmat.2015.07.186.
[38] J. Trägårdh, F. Bellmann, Sulphate attack., RILEM Rep. 38 (2007) 89–118. https://doi.org/10.1160/TH14-11-0977.
[39] E. Menéndez-Mendez, T. Matschei, F.P. Glasser, Sulfate Attack of Concrete, in: M. Alexander, A. Bertron, N. De Belie (Eds.), Perform. Cem. Mater. Aggress. Aqueous Environ., RILEM, Springer, 2013: pp. 8–74. https://doi.org/10.1007/978-94-007-5413-3.
[40] H. Haynes, R. O'Neill, K.P. Mehta, Concrete Deterioation from Physical Attack by Salts, Concr. Int. 18 (1996) 63–68.
[41] G.W. Scherer, Stress from crystallization of salt, Cem. Concr. Res. 34 (2004) 1613–1624. https://doi.org/10.1016/j.cemconres.2003.12.034.
[42] A. Neville, The confused world of sulfate attack on concrete, Cem. Concr. Res. 34 (2004) 1275–1296. https://doi.org/10.1016/j.cemconres.2004.04.004.
[43] M. Whittaker, L. Black, Current knowledge of external sulfate attack, Adv. Cem. Res. 27 (2015) 532–545. https://doi.org/10.1680/adcr.14.00089.
[44] M.F. Suma, M. Santhanam, Influence of the specimen size on the expansion of Portland cement mortar immersed in sodium sulphate solution, in: E. Menéndez-Mendez, V. Baroghel-Bouny (Eds.), Extern. Sulfate Attack - F. Asp. Lab Tests, RILEM Book, Springer, 2020: p. 163.
[45] H.M. Rietveld, A profile method for nuclear and magnetic structures, J. Appl. Cystallogr. 2 (1969) 65–71.
[46] IRAM, IRAM 1622. Cemento Pórtland. Métodos de determinación de las resistencias a la compresión y a la flexión., 1962.
[47] ACI, ACI 318 - Building Code Requirements for Structural Concrete and Commentary, 2019.
[48] B. Lothenbach, P. Durdzinski, K. De Weerdt, Thermogravimetric analysis, in: K. Scrivener, R. Snellings, B. Lothenbach (Eds.), A Pract. Guid. to Microstruct. Anal. Cem. Mater., 1st ed., CRC Press, Boca Raton, USA, 2016: pp. 177–211.
[49] L. Evangelista, J. de Brito, Durability performance of concrete made with fine recycled concrete aggregates, Cem. Concr. Compos. 32 (2010) 9–14. https://doi.org/10.1016/j.cemconcomp.2009.09.005.
[50] ASTM, ASTM C 1012 - Standard Test Method for Length Change of Hydraulic-Cement Mortars Exposed to a Sulfate Solution, n.d.
[51] R. El-Hachem, E. Rozire, F. Grondin, A. Loukili, New procedure to investigate external sulphate attack on cementitious materials, Cem. Concr. Compos. 34 (2012) 357–364. https://doi.org/10.1016/j.cemconcomp.2011.11.010.
[52] S. Lee, Influence of recycled fine aggregates on the resistance of mortars to magnesium sulfate attack, Waste Manag. 29 (2009) 2385–2391. https://doi.org/10.1016/j.wasman.2009.04.002.
[53] W. Müllauer, R.E. Beddoe, D. Heinz, Sulfate attack expansion mechanisms, Cem. Concr. Res. 52 (2013) 208–215. https://doi.org/10.1016/j.cemconres.2013.07.005.

[54] S. Messad, M. Carcassès, L. Linger, L. Boutillon, Performance Approach Using Accelerated Test Method for External Sulfate Attack, Third Int. Fib Congr. (2010) 1–11.
[55] E.F. Irassar, V.L. Bonavetti, M. González, Microstructural study of sulfate attack on ordinary and limestone Portland cements at ambient temperature, Cem. Concr. Res. 33 (2003) 31–41. https://doi.org/10.1016/S0008-8846(02)00914-6.
[56] C. Yu, W. Sun, K. Scrivener, Degradation mechanism of slag blended mortars immersed in sodium sulfate solution, Cem. Concr. Res. 72 (2015) 37–47. https://doi.org/10.1016/j.cemconres.2015.02.015.
[57] M. Etxeberria, E. Vázquez, A. Marí, Microstructure analysis of hardened recycled aggregate concrete, Mag. Concr. Res. 58 (2006) 683–690. https://doi.org/10.1680/macr.2006.58.10.683.
[58] N.N. Naik, A.C. Jupe, S.R. Stock, A.P. Wilkinson, P.L. Lee, K.E. Kurtis, Sulfate attack monitored by microCT and EDXRD: Influence of cement type, water-to-cement ratio, and aggregate, Cem. Concr. Res. 36 (2006) 144–159. https://doi.org/10.1016/j.cemconres.2005.06.004.
[59] S. Candamano, F. Tassone, I. Iacobini, F. Crea, P. De Fazio, applied sciences The Properties and Durability of Self-Leveling and Thixotropic Mortars with Recycled Sand, Appl. Sci. (2022) 2732.
[60] B. Qi, J. Gao, F. Chen, D. Shen, Evaluation of the damage process of recycled aggregate concrete under sulfate attack and wetting-drying cycles, Constr. Build. Mater. 138 (2017) 254–262. https://doi.org/10.1016/j.conbuildmat.2017.02.022.
[61] F. Li, C. Li, S. Zhao, C. Shi, Concrete deterioration under alternate action of carbonation and sulfate attack, Res. J. Appl. Sci. 6 (2013) 3736–3740.